Improved Multiplicative Regularization for CSI-EPT

Helfferich, Florens; Van Den Berg, Peter M.; Remis, Rob F.

DOI
10.1109/JERM.2024.3363428

Publication date
2024

Document Version
Final published version

Published in
IEEE Journal of Electromagnetics, RF and Microwaves in Medicine and Biology

Improved Multiplicative Regularization for CSI-EPT

Florens Helfferich, Peter M. van den Berg, and Rob F. Remis

***Abstract*—We present an improved multiplicative Contrast Source Inversion (CSI) approach for Electrical Properties Tomography (EPT). In EPT, the conductivity and permittivity profiles of a body part are reconstructed based on a known circularly polarized part of the magnetic field (the B_1^+-field) that has its support inside the body part of interest. The CSI method attempts to reconstruct these profiles in an iterative and alternating manner by first fixing the contrast and updating the contrast source (product of tissue contrast and electric field) and subsequently fixing the contrast source and updating the contrast. In this paper, regularization is included in a multiplicative way similar to the standard multiplicative CSI-EPT method. However, the regularized objective function is different and an update for the contrast is obtained through one-step Jacobi filtering of a least-squares reconstruction that is based on the updated contrast source. Two-dimensional numerical experiments for conductivity and permittivity tissue profiles of a female body model show that, for data with various noise levels, the proposed regularization approach generally provides improved tissue reconstructions compared with standard multiplicative CSI-EPT.**

***Index Terms*—B_1^+ field, electrical properties tomography, magnetic resonance imaging, multiplicative contrast source inversion.**

I. Introduction

ELECTRICAL Properties Tomography or EPT is a hybrid inverse scattering problem in Magnetic Resonance Imaging (MRI) in which the objective is to reconstruct the conductivity and permittivity profiles of a body part of interest [1], [2]. Based on the left-handed circularly polarized part of the magnetic field that is known at the Larmor frequency *inside* the body part of interest (EPT is a so-called hybrid inverse problem with data supported inside the reconstruction domain), reconstruction methods attempt to retrieve the dielectric tissue profiles. Knowledge about the conductivity and permittivity of tissue is of great importance in MR safety [3], [4], [5], hyperthermia treatment planning [6], and stroke imaging [7], for example.

A wide variety of EPT reconstruction approaches have been developed each with its own advantages and disadvantages. We refer to [8] for an overview of these methods and to [9] and [10] as examples of recent learning-based EPT reconstruction methods. In this paper, we focus on the Contrast Source Inversion (CSI) method, which was proposed in [11] for remote sensing problems, applied to various inverse scattering problems in [12], [13], and [14] for example, and applied to the EPT problem in [15]. In particular, we consider a specific one-step Jacobi multiplicative regularization approach for CSI, which was originally proposed for remote sensing problems in [16]. We apply this approach to the EPT problem and demonstrate that it generally provides improved EPT reconstructions of a body part of interest compared with standard multiplicative CSI as obtained in [17], for example, where the effects of various modeling errors in CSI-EPT are discussed as well. The regularization step is noniterative and consists of a simple one-step Jacobi correction of the inverted least-squares contrast. Furthermore, similar to the original multiplicative regularization scheme, no regularization parameter needs to be determined for each new data set and, finally, the computational costs are similar to the costs of the original multiplicative CSI method.

This paper is organized as follows. In Section II we briefly review the basic equations for CSI-EPT. The standard CSI-EPT method and the standard multiplicative CSI-EPT scheme are reviewed in Section III, while the one-step Jacobi regularization approach is presented in Section IV. In Section V we present numerical experiments that demonstrate the effectiveness of the new regularization approach and the conclusions can be found in Section VI.

II. Basic Equations

Let us first briefly present the basic equations that govern our 2D EPT problem. We consider an E-polarized RF field in a configuration that is invariant in the z-direction. A penetrable body part of interest, characterized by a conductivity σ and a permittivity ε, occupies a bounded domain $\mathbb{D}$ in the xy-plane and is embedded in free space. In EPT, the problem is to reconstruct the conductivity and permittivity profiles of the body from a known circularly polarized part of the magnetic field *inside* the body. This part of the magnetic field is called the B_1^+-field and since the B_1^+-field is known inside the reconstruction domain $\mathbb{D}$, the EPT reconstruction problem is what is called a hybrid inverse problem.

A set of line sources (representing the rungs of a birdcage coil) surrounds the object under test (see also Fig. 1 below). The electric field generated by these sources when the object is absent is denoted as the incident field u^{inc}, while the field that is present when the object is present is denoted as the total field u. The scattered field $u^{\text{sc}} = u - u^{\text{inc}}$ is introduced as the difference

Manuscript received 25 October 2023; revised 13 January 2024; accepted 1 February 2024. Date of publication 16 February 2024; date of current version 1 March 2024. *(Corresponding author: Rob F. Remis.)*

Florens Helfferich is with the Faculty of Electrical Engineering, Mathematics, and Computer Science, Delft University of Technology, 2628 CD Delft, The Netherlands.

Peter M. van den Berg is with the Delft University of Technology, 2628 CD Delft, The Netherlands.

Rob F. Remis is with the Terahertz Sensing Group of the Faculty of Electrical Engineering, Mathematics, and Computer Science, Delft University of Technology, 2628 CD Delft, The Netherlands (e-mail: R.F.Remis@tudelft.nl).

Digital Object Identifier 10.1109/JERM.2024.3363428

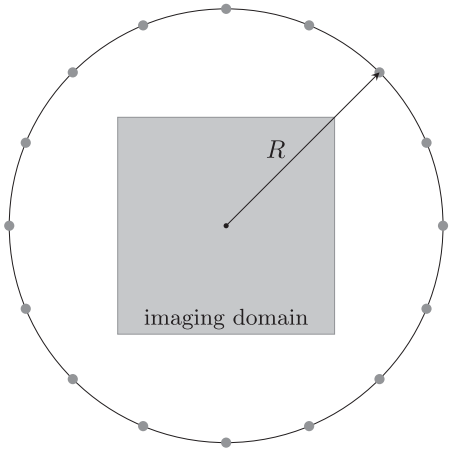

Fig. 1. Sixteen line sources (gray dots) representing the rungs of a birdcage coil. The line sources are equally distributed on a circle with a radius $R = 0.352$ m.

between the total and incident field and for this scattered field we have the integral representation

$$u^{\text{sc}}(\mathbf{x}) = k_0^2 \int_{\mathbf{x}' \in \mathbb{D}} G(\mathbf{x} - \mathbf{x}') \chi(\mathbf{x}') u(\mathbf{x}') \, \mathrm{d}V, \tag{1}$$

which holds for $\mathbf{x} \in \mathbb{R}^2$. In the above equation, $k_0 = \omega / c_0$ is the wave number of the background medium, where c_0 is the electromagnetic wave speed of the background, $G(\mathbf{x}) = -\frac{\mathrm{j}}{4} H_0^{(2)}(k_0 |\mathbf{x}|)$ is the Green's function with $H_0^{(2)}$ the Hankel function of the second kind and order zero, and χ is the contrast function of the object given by

$$\chi(\mathbf{x}) = \varepsilon_{\text{r}}(\mathbf{x}) - 1 - \mathrm{j} \frac{\sigma(\mathbf{x})}{\omega \varepsilon_0} \tag{2}$$

with ε_{r} the relative permittivity of the object and σ its conductivity.

The input data of CSI-EPT is the scattered B_1^+-field within the domain of interest $\mathbb{D}$, which we denote by $d(\mathbf{x})$. From Maxwell's equations it follows that for this scattered field data we have the representation

$$d(\mathbf{x}) = \frac{1}{2\omega} \partial^+ u^{\text{sc}} = \frac{\omega}{2c_0^2} \partial^+ \int_{\mathbf{x}' \in \mathbb{D}} G(\mathbf{x} - \mathbf{x}') \chi(\mathbf{x}') u(\mathbf{x}') \, \mathrm{d}V \tag{3}$$

for $\mathbf{x} \in \mathbb{D}$, where $\partial^+ = \partial_x + \mathrm{j} \partial_y$. We write the above expression for the data more compactly as

$$d = \mathcal{G}_{\text{d}} w, \tag{4}$$

where $w = \chi u$ is the contrast source and $\mathcal{G}_{\text{d}}$ the data operator given by

$$\mathcal{G}_{\text{d}} w = \frac{\omega}{2c_0^2} \partial^+ \int_{\mathbf{x}' \in \mathbb{D}} G(\mathbf{x} - \mathbf{x}') w(\mathbf{x}') \, \mathrm{d}V \tag{5}$$

with $\mathbf{x} \in \mathbb{D}$. Equation (4) is referred to as the data equation. Finally, using the definition of the scattered field $u^{\text{sc}} = u - u^{\text{inc}}$ in (1), restricting the observation vector to the domain of interest $\mathbb{D}$, and multiplying by the contrast χ, we arrive at the object or state equation

$$w - \chi \mathcal{G}_{\text{o}} w = \chi u^{\text{inc}}, \tag{6}$$

with $\mathbf{x} \in \mathbb{D}$, where we have introduced the object operator as

$$\mathcal{G}_{\text{o}} w = k_0^2 \int_{\mathbf{x}' \in \mathbb{D}} G(\mathbf{x} - \mathbf{x}') w(\mathbf{x}') \, \mathrm{d}V, \quad \mathbf{x} \in \mathbb{D}. \tag{7}$$

With the introduction of the data and object equations and operators, we are in a position to discuss the CSI-EPT reconstruction algorithm.

III. Contrast Source Inversion

Suppose that the body part of interest that occupies the domain $\mathbb{D}$ is illuminated by RF fields due to $N_{\text{ex}} \geq 1$ different coil excitations. For the ith excitation, we then have the data and object equation

$$d_i = \mathcal{G}_{\text{d}} w_i \quad \text{and} \quad w_i - \chi \mathcal{G}_{\text{o}} w_i = \chi u_i^{\text{inc}}, \tag{8}$$

for $i = 1, 2, \ldots, N_{\text{ex}}$, respectively.

To measure the discrepancy in satisfying the data and object equations for arbitrary contrasts χ and contrast sources w_i, we introduce the data and object residuals as

$$r_{\text{d};i} = d_i - \mathcal{G}_{\text{d}} w_i \quad \text{and} \quad r_{\text{o};i} = \chi u_i^{\text{inc}} - w_i + \chi \mathcal{G}_{\text{o}} w_i, \tag{9}$$

for $i = 1, 2, \ldots, N_{\text{ex}}$, respectively. We note that since the total field u_i inside the object domain is given by $u_i = u_i^{\text{inc}} + G_{\text{o}} w_i$, the object residual can also be written as

$$r_{\text{o};i} = \chi u_i - w_i, \tag{10}$$

for $i = 1, 2, \ldots, N_{\text{ex}}$. The magnitude of these residuals is measured using the Euclidean norm $\| \cdot \|$ defined on the reconstruction domain $\mathbb{D}$.

In CSI-EPT, the contrast and contrast sources are updated in an iterative manner. In particular, at the nth iteration we assume that we have an approximate contrast $\chi^{[n-1]}$ and contrast sources $w_i^{[n-1]}$ available and the objective function

$$F^{[n]}(\chi, w) = F^{\text{data}}(w) + F^{\text{object}}(\chi, w | \chi^{[n-1]}) \tag{11}$$

is considered, where

$$F^{\text{data}}(w) = \eta_{\text{d}} \sum_{i=1}^{N_{\text{ex}}} \| r_{\text{d};i} \|^2 \tag{12}$$

with $\eta_{\text{d}} = 1 / \sum_{i=1}^{N_{\text{ex}}} \| d_i \|^2$ measures the magnitude of the data mismatch. Note that $F^{\text{data}}(w)$ is shorthand notation for $F^{\text{data}}(w_1, w_2, \ldots, w_{N_{\text{ex}}})$.

Furthermore, the object objective function is defined as

$$F^{\text{object}}(\chi, w | \chi^{[n-1]}) = \eta_{\text{o}}^{[n-1]} \sum_{i=1}^{N_{\text{ex}}} \| r_{\text{o};i} \|^2 \tag{13}$$

with $\eta_{\text{o}}^{[n-1]} = 1 / \sum_{i=1}^{N_{\text{ex}}} \| \chi^{[n-1]} u_i^{\text{inc}} \|^2$ and measures the magnitude of the object equation mismatch.

The contrast and contrast source are now updated in a two step procedure. In particular, at the nth iteration, first the contrast is fixed to the current estimate $\chi = \chi^{[n-1]}$ and the contrast sources are updated using the update formula

$$w_i^{[n]} = w_i^{[n-1]} + \alpha_i^{[n]} p_i^{[n]}, \quad \text{for } i = 1, 2, \ldots, N_{\text{ex}}, \tag{14}$$

where $p_i^{[n]}$ are the Polak-Ribière update directions. These directions are determined in terms of the gradients of $F^{[n]}(\chi^{[n-1]}, w)$

with respect to w. Explicit expressions for the update coefficients and update directions can be found in [16], for example.

Second, the contrast is updated by minimizing $F^{[n]}(\chi, w^{[n]})$ with respect to χ. Using the alternate expression for $r_{o;i}$ as given by (10), this minimum is easily found as

$$\chi^{[n]} = \frac{\sum_{i=1}^{N_{ex}} w_i^{[n]} u_i^{[n]*}}{\sum_{i=1}^{N_{ex}} |u_i^{[n]}|^2}, \tag{15}$$

where $u_i^{[n]} = u_i^{inc} + \mathcal{G}_o w_i^{[n]}$, $i = 1, 2, \ldots, N_{ex}$, and the asterisk denotes complex conjugation. The contrast and contrast source now have both been updated and the CSI-EPT algorithm continues with the next iteration.

A. Contrast Source Inversion With Multiplicative Regularization

In the original regularized CSI method, regularization is included in a multiplicative manner and the objective function

$$F_{MR}^{[n]}(\chi, w) = F^{[n]}(\chi, w) F_R(\chi|\chi^{[n-1]}), \tag{16}$$

is considered at the nth iteration instead of objective function (11). In the above expression, $F_R(\chi|\chi^{[n-1]})$ is the multiplicative regularization function given by

$$F_R(\chi|\chi^{[n-1]}) = \frac{1}{A}\int_{x\in\mathbb{D}} \frac{|\nabla\chi|^2 + \delta^{[n-1]}}{|\nabla\chi^{[n-1]}|^2 + \delta^{[n-1]}}\, dV \tag{17}$$

with A the area of the domain $\mathbb{D}$ and

$$\delta^{[n-1]} = (1/\Delta^2) F^{object}\left(\chi^{[n-1]}, w^{[n]}\middle|\chi^{[n-1]}\right), \tag{18}$$

where Δ is the side length of a pixel used when discretizing the object domain $\mathbb{D}$.

Note that, by construction, $F_R(\chi^{[n-1]}|\chi^{[n-1]}) = 1$ and therefore the presence of F_R does not affect the updating procedure for the contrast sources w_i. The update procedure for the contrast does change, however. Explicitly, we update the contrast according to the formula

$$\chi^{[n]} = \chi_{csi}^{[n]} + \beta^{[n]} q^{[n]}, \tag{19}$$

where $\chi_{csi}^{[n]}$ is the contrast of (15) and $q^{[n]}$ is the Polak-Ribière update direction expressed in terms of the gradient of $F_{MR}^{[n]}(\chi, w^{[n]})$ with respect to χ. Explicit expressions for the update direction and the gradient can be found in [17], where it is also shown how to compute the update coefficient $\beta^{[n]}$. The performance of this type of regularization has been extensively demonstrated for CSI and CSI-EPT in [14] and [17], respectively.

IV. One-Step Jacobi Contrast Inversion

At the nth iteration of the improved multiplicative regularization approach followed in this paper, we first update the contrast sources w_i just as in standard CSI or the multiplicative CSI method of the previous section. In other words, updating the contrast sources is the same as in standard (multiplicative) CSI. Having updated these contrast sources, the corresponding total fields $u_i^{[n]}$ are determined and the contrast $\chi_{csi}^{[n]}$ estimate of (15) is computed. Subsequently, the objective function

$$F_{MR}^{[n]}(\chi, w^{[n]}) = \left[F^{data}(w^{[n]}) + \frac{\int_{x\in\mathbb{D}} |\chi - \chi_{csi}^{[n]}|^2\, dV}{\int_{x\in\mathbb{D}} |\chi_{csi}^{[n]}|^2\, dV}\right] F_R\left(\chi|\chi_{csi}^{[n]}\right), \tag{20}$$

is considered with

$$F_R\left(\chi|\chi_{csi}^{[n]}\right) = \frac{1}{A}\int_{x\in\mathbb{D}} \frac{|\nabla\chi|^2 + \delta^{[n]}}{|\nabla\chi_{csi}^{[n]}|^2 + \delta^{[n]}}\, dV \tag{21}$$

and

$$\delta^{[n]} = (1/\Delta^2) F^{object}\left(\chi_{csi}^{[n]}, w^{[n]}\middle|\chi_{csi}^{[n]}\right). \tag{22}$$

Finally, the updated contrast is obtained as

$$\chi^{[n]} = \underset{\chi}{\operatorname{argmin}}\, F_{MR}\left(\chi, w^{[n]}\right). \tag{23}$$

Minimization of F_{MR} is carried out by calculating the first variation of this function with respect to $\chi^*(\mathbf{x})$ with $\mathbf{x} \in \mathbb{D}$ (see [16]). We then arrive at the Euler-Lagrange equation that corresponds to this minimization problem. This is a nonlinear equation in χ, but to find a regularized contrast it is sufficient to only consider the linearized Euler-Lagrange equation, which is given by [16]

$$\chi(\mathbf{x}) - \left[F^{data}(w^{[n]}) M\left(\chi_{csi}^{[n]}\right)\right] \boldsymbol{\nabla} \cdot \left[b^{[n]} \boldsymbol{\nabla}\chi(\mathbf{x})\right] = \chi_{csi}^{[n]}(\mathbf{x}) \tag{24}$$

with $\mathbf{x} \in \mathbb{D}$. In the above equation

$$b^{[n]} = \left(\left|\boldsymbol{\nabla}\chi_{csi}^{[n]}\right|^2 + \delta^{[n]}\right)^{-1} \tag{25}$$

and $M(\chi_{csi}^{[n]})$ is the mean of $|\chi_{csi}^{[n]}|^2$ over the domain $\mathbb{D}$ given by

$$M\left(\chi_{csi}^{[n]}\right) = \frac{1}{A}\int_{\mathbf{x}\in\mathbb{D}} \left|\chi_{csi}^{[n]}\right|^2 dV \tag{26}$$

with $A = \int_{\mathbf{x}\in\mathbb{D}} dA$ the area of the domain $\mathbb{D}$.

In practice, (24) is discretized on a uniform grid with pixels having a side length Δ and using two-point finite-difference formulas for the gradient and divergence operators. After this discretization procedure (for details, see [16]), we arrive at a system of equations $\mathsf{A}\mathsf{c} = \mathsf{c}_{csi}^{[n]}$, where c and $\mathsf{c}_{csi}^{[n]}$ are the discretized and vectorized counterparts of χ and $\chi_{csi}^{[n]}$, respectively. Moreover, it can be shown that matrix A is diagonally dominant and therefore a new contrast is computed by carrying out a single Jacobi iteration with $\mathsf{c}_{csi}^{[n]}$ as initial guess. Explicitly, the new contrast is computed from $\mathsf{c}_{csi}^{[n]}$ as

$$\mathsf{c}^{[n]} = \mathsf{D}^{-1}(\mathsf{I} - \mathsf{R})\mathsf{c}_{csi}^{[n]}, \tag{27}$$

where D is the diagonal of matrix A and $\mathsf{R} = \mathsf{A} - \mathsf{D}$ the remainder. The new contrast has now been determined and CSI proceeds to the next iteration.

V. Numerical Experiments

We demonstrate the performance of the proposed regularization approach by considering tissue profiles through the pelvis

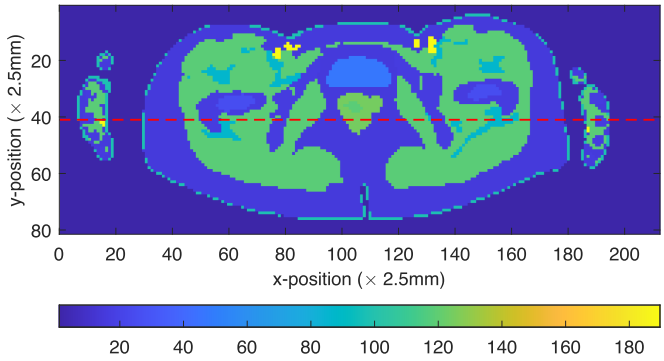

Fig. 2. Magnitude plot of the contrast χ at 128 MHz of a slice through the pelvis region of the Ella model of the ITIS foundation. The dashed line indicates the position of the line profiles shown in Figs. 4 and 6.

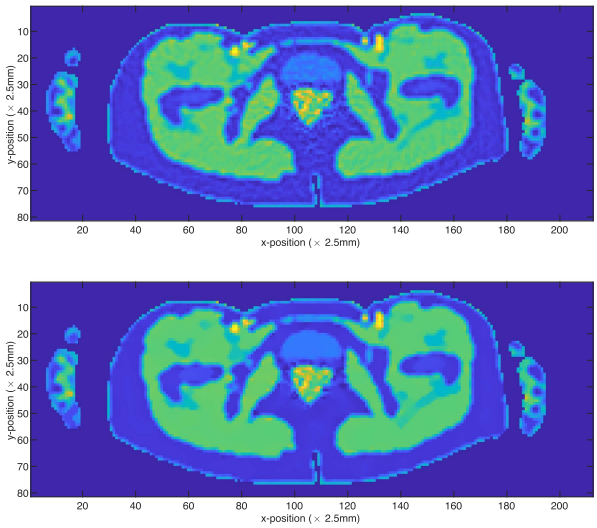

Fig. 3. Magnitude of the reconstructed contrast after 1000 iterations of the standard multiplicative CSI-EPT method (top) and Jacobi multiplicative CSI-EPT method (bottom) for B_1^+- amplitude and phase data with an SNR of 50 dB.

region and head of the Ella body model of the ITIS foundation [18]. The profiles are located within the imaging domain, which is surrounded by 16 line sources representing the rungs of an RF coil, see Fig. 1. The line sources are uniformly distributed on a circle with a radius of 0.352 m. Its center coincides with the center of the imaging domain. The line sources operate at a Larmor frequency of 128 MHz, which corresponds to an MR background field of 3 T. The conductivity and permittivity values of the various tissue types within the slice through the pelvis region at 128 MHz are taken from the ITIS database. A magnitude plot of the corresponding contrast profile is shown in Fig. 2. Finally, the same three coil excitations (one quadrature and two linear excitations) as in [15] are used to illuminate the pelvis region of the body.

Subsequently, for the given coil excitations, the B_1^+ field inside the pelvis region is computed and the magnitudes and phases of these fields are contaminated by random Gaussian noise such that the resulting B_1^+ amplitudes and phases have a signal to noise ratio of 40 or 50 dB [19]. These noisy data sets now serve as input for the multiplicative CSI-EPT algorithms.

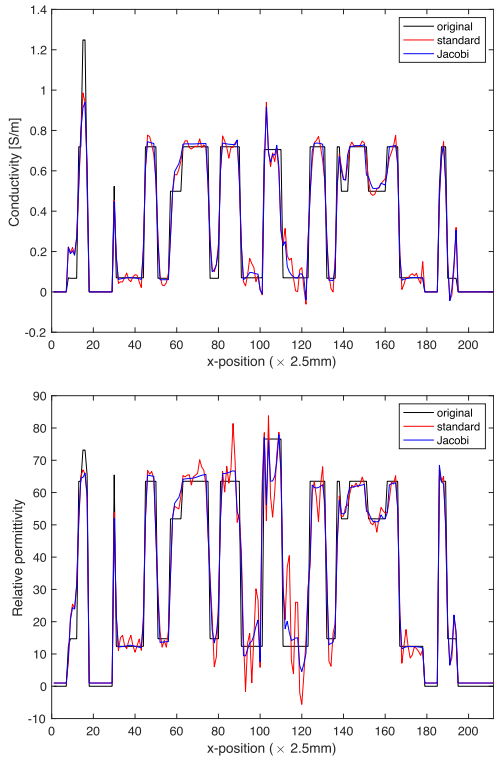

Fig. 4. Conductivity and relative permittivity profiles on the line illustrated in Fig. 2. The exact conductivity and permittivity profiles are shown (black lines) along with the reconstructed profiles for standard CSI-EPT (red line) and Jacobi CSI-EPT (blue line). Reconstructions were obtained for 50 dB noisy B_1^+-data.

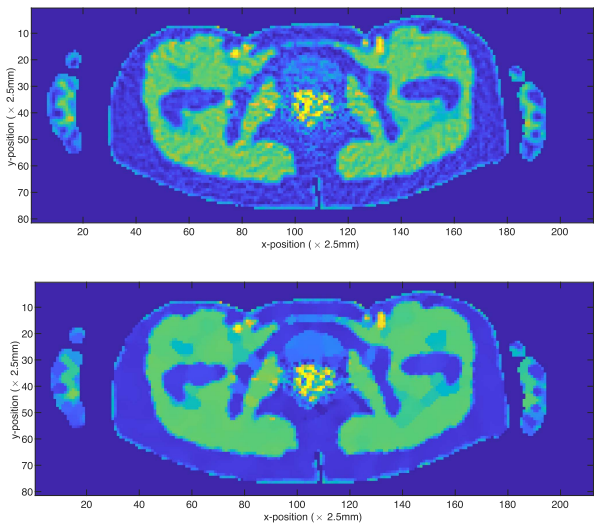

Fig. 5. Magnitude of the reconstructed contrast after 1000 iterations of the standard multiplicative CSI-EPT method (top) and Jacobi multiplicative CSI-EPT method (bottom) for B_1^+-amplitude and phase data with an SNR of 40 dB.

The magnitude of the reconstructed contrast profile after 1000 iterations is shown in Fig. 3 (top) and 3 (bottom) for the standard and one-step Jacobi multiplicative CSI-EPT method and 50 dB noisy B_1^+-data, respectively. The Structural Similarity Index Measure (SSIM) for the reconstructed magnitude of the contrast

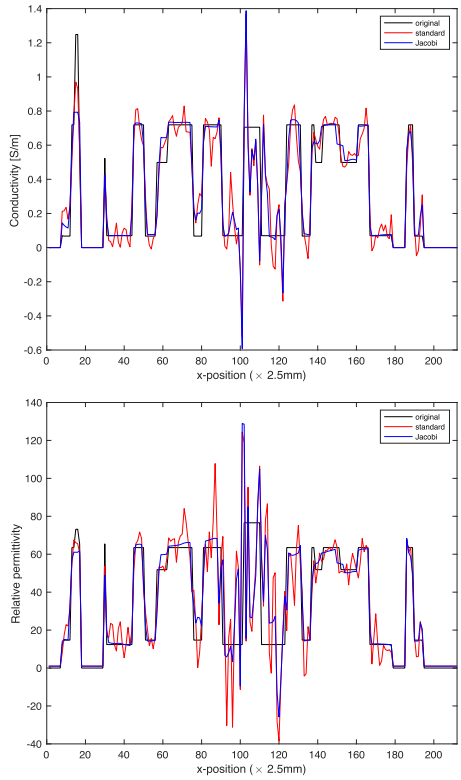

Fig. 6. Conductivity and relative permittivity profiles on the line illustrated in Fig. 2. The exact conductivity and permittivity profiles are shown (black lines) along with the reconstructed profiles for standard CSI-EPT (red line) and Jacobi CSI-EPT (blue line). Reconstructions were obtained for 40 dB noisy B_1^+-data.

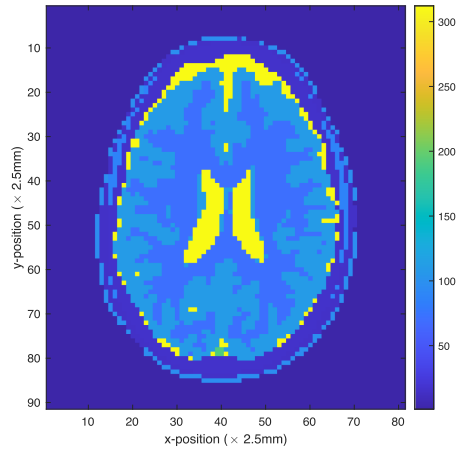

Fig. 7. Magnitude of the contrast tissue model of the head of the Ella body model at 128 MHz.

is 0.3587 for standard multiplicative CSI-EPT and 0.3742 for the proposed Jacobi variant.

We observe that noise is much better suppressed by Jacobi CSI-EPT than standard CSI-EPT. Also note that for both approaches, the reconstructions in the middle of the profile are the least accurate. This is due to a small electric field that is present around the center of the profile (see also [15]). Furthermore,

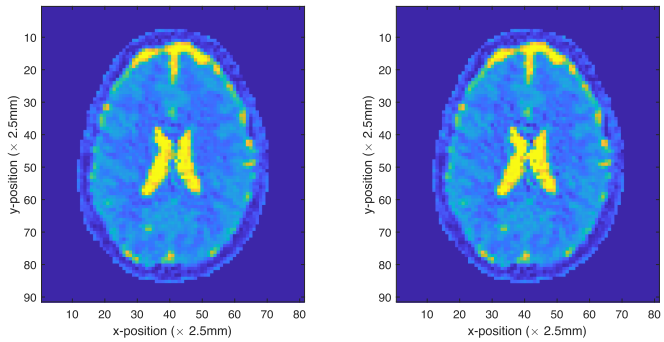

Fig. 8. Magnitude of the reconstructed contrast after 1000 iterations of the standard multiplicative CSI-EPT method (left) and Jacobi multiplicative CSI-EPT method (right) for B_1^+-amplitude and phase data with an SNR of 40 dB.

in Fig. 4 the reconstructed conductivity (top) and permittivity (bottom) profiles on the dashed line of Fig. 2 are shown. Reconstruction results for standard (red line) and one-step Jacobi (blue line) are shown. Clearly, improved reconstructions are obtained with one-step Jacobi CSI-EPT. The large jumps in the conductivity and permittivity profiles are also essentially captured by the CSI-EPT reconstructions.

In Fig. 5 reconstruction results after 1000 iterations of standard (top, SSIM = 0.3172) and Jacobi CSI-EPT (bottom, SSIM = 0.3452) are shown for 40 dB B_1^+-data. Again, noise is much better suppressed by the Jacobi CSI-EPT method and the difference between the original multiplicative approach and the Jacobi approach is even more dramatic. The line profiles of Fig. 6 also illustrate this, where in the top figure the reconstructed conductivity on the dashed line of Fig. 2 is shown, while the reconstructed permittivity is shown in the bottom figure. Also note that since the magnitude of the electric field is small at the center of the slice, the effects due to noise are much more severe at this location for 40 dB data than for 50 dB data. Finally, we mention that the computational complexity of a single iteration of each method is of approximately the same order and one-step Jacobi regularization therefore provides improved reconstructions of noisy data for the pelvis region at approximately the same computational costs. Specifically, for the pelvis region the reconstruction time of standard and Jacobi regularization is approximately four minutes on a standard laptop with a 2 GHz Intel Core i7-8565 U CPU, 8 GB RAM, and running Matlab 2022b.

As a last example, we consider the contrast profile of a slice through the head of the Ella body model as illustrated in Fig. 7. Such a profile is also considered in [20] and [21]. The reconstructions obtained for noisy 40 dB B_1^+ data with standard and Jacobi multiplicative regularization are shown in Fig. 8 (left) and 8 (right), respectively. In this case, magnitude reconstructions using standard and Jacobi regularization take about one minute on the same computer as mentioned above and both reconstructions have an SSIM of about 0.45. Visual inspection of the reconstructions shown in Fig. 8 also confirms that both reconstructions are indeed very similar. In this case, Jacobi regularization provides a reconstruction of a similar

quality as standard regularization. Further experiments indicate that for the EPT problem considered here, Jacobi regularization generally provides reconstructions that are of at least the same quality as standard multiplicative regularization.

VI. Conclusion

In this paper, we have presented a multiplicative CSI-EPT method to suppress the effects of noise on CSI-EPT reconstructions. The method considers the contrast source and contrast as fundamental unknowns and updates these quantities in an alternating manner. Specifically, at each iteration, first the contrast is fixed and the contrast source is updated (step 1) and subsequently the contrast source is fixed and the contrast is updated (step 2). In the first step, the contrast source is updated in the same manner as in standard CSI-EPT and this updated contrast source provides us with a least-squares reconstruction of the contrast. The second step, however, is different and filters the least-squares reconstruction of the first step by carrying out a single Jacobi iteration on an equation that follows from approximately minimizing a multiplicative objective function for the contrast. By construction, this objective function suppresses noise in the contrast (tissue) reconstructions.

For noisy 40 dB or 50 dB B_1^+ data, we have illustrated the performance of the one-step Jacobi approach and compared the reconstruction results with reconstructions obtained with standard multiplicative CSI-EPT. A strongly inhomogeneous slice through the pelvis region and the head of a female body model were used for the comparison. Reconstruction results were presented that show that one-step Jacobi generally provides improved noise compression compared with standard CSI-EPT. Furthermore, the action of the discretized integral operators in CSI-EPT can be computed using FFTs, since the spatial grid is uniform. Moreover, differentiation in the regularization operator is implemented using two-point finite differences and consequently the computational costs of a CSI-EPT iteration is dominated by FFTs. For the head and pelvis region it typically takes around 500 (head) to 1000 (pelvis) iterations to match the data to noise level and computation times in Matlab are in the order of minutes on a standard laptop. Finally, no regularization parameters need to be determined (computed) in multiplicative CSI-EPT, but its performance does depend on the noise level, the choice for $\delta^{[n]}$, and how the finite-differences are implemented. Different implementations may also require a different number of CSI-EPT iterations to reach a satisfactory reconstruction.

Nevertheless, given the promising reconstruction results for 2D tissue profiles, we intend to extend Jacobi regularization to 3D CSI-EPT [22]. Moreover, the presence of the RF shield in the background should be taken into account. Finally, we have assumed that the phase of the B_1^+ field is known. In practice, however, this phase is not directly measurable and only approximately known [23]. Using the technique presented in [23], it may be possible to reconstruct the phase during the iteration process and it is our objective to incorporate one-step Jacobi noise suppression in this technique as well.

References

[1] U. Katscher and C. A. T. van den Berg, "Electric properties tomography: Biochemical, physical and technical background, evaluation and clinical applications," *NMR Biomed.*, vol. 30, no. 8, pp. 1–15, 2017.

[2] J. Liu, Y. Wang, U. Katscher, and B. He, "Electrical properties tomography based on B_1 maps in MRI: Principles, applications, and challenges," *IEEE Trans. Biomed. Eng.*, vol 64, no. 11, pp. 2515–2530, Nov. 2017.

[3] J. Chen, Z. Feng, and J. M. Jin, "Numerical simulation of SAR and B1-field inhomogeneity of shielded RF coils loaded with the human head," *IEEE Trans. Biomed. Eng.*, vol. 45, no. 5, pp. 650–659, May 1998.

[4] U. Katscher, T. Voigt, C. Findeklee, P. Vernickel, K. Nehrke, and O. Dössel, "Determination of electrical conductivity and local SAR via B1 mapping," *IEEE Trans. Med. Imag.*, vol. 28, no. 9, pp. 1365–1374, Sep. 2009.

[5] C. M. Collins et al., "Temperature and SAR calculations for a human head within volume and surface coils at 64 and 300 MHz," *J. Magn. Reson. Imag.*, vol. 19, no. 5, pp. 650–656, 2004.

[6] E. Balidemaj et al., "B1-based SAR reconstruction using contrast source inversion - electric properties tomography (CSI-EPT)," *Med. Biol. Eng. Comput.*, vol. 55, no. 2, pp. 225–233, 2017.

[7] L. X. Liu et al., "A new method of non-invasive brain-edema monitoring in stroke: Cerebral electrical impedance measurement," *Neurological Res.*, vol. 28, no. 1, pp. 31–37, 2006.

[8] R. Leijsen, W. Brink, C. van den Berg, A. Webb, and R. Remis, "Electrical properties tomography: A methodological review," *Diagnostics*, vol. 11, no. 2, 2021, Art. no. 176.

[9] A. J. G. Inda et al., "Physics informed neural networks (PINN) for low Snr magnetic resonance electrical properties tomography (MREPT)," *Diagnostics*, vol. 12, no. 11, 2022, Art. no. 2627.

[10] R. Leijsen, C. van den Berg, A. Webb, R. Remis, and S. Mandija, "Combining deep learning and 3D contrast source inversion in MR-based electrical properties tomography," *NMR Biomed.*, vol. 35, no. 4, 2022, Art. no. e4211.

[11] P. M. van den Berg and R. E. Kleinman, "A contrast source inversion method," *Inverse Problems*, vol. 13, no. 6, pp. 1607–1620, 1997.

[12] P. M. van den Berg, A. Abubakar, and J. T. Fokkema, "Multiplicative regularization for contrast profile inversion," *Radio Sci.*, vol. 38, no. 2, pp. 23-1–23-10, Apr. 2003.

[13] A. Abubakar, P. M. van den Berg, and J. J. Mallorqui, "Imaging of biomedical data using a multiplicative reularized contrast source inversion method," *IEEE Trans. Microw. Theory Techn.*, vol. 50, no. 7, pp. 1761–1771, Jul. 2002.

[14] A. Abubakar, P. M. van den Berg, and T. M. Habashy, "Application of the multiplicative regularized contrast source inversion method on TM- and TE-polarized experimental fresnel data," *Inverse Problems*, vol. 21, no. 6, pp. S5–S13, 2005.

[15] E. Balidemaj et al., "CSI-EPT: A contrast source inversion approach for improved MRI-based electrical properties tomography," *IEEE Trans. Med. Imag.*, vol. 34, no. 9, pp. 1788–1796, Sep. 2015.

[16] P. M. van den Berg, *Forward and Inverse Scattering Algorithms Based on Contrast Source Integral Equations*, Hoboken, NJ, USA: Wiley, 2021.

[17] R. L. Leijsen, W. M. Brink, A. G. Webb, and R. F. Remis, "Effects of simulated error sources on different 3-D CSI-EPT strategies," *IEEE Trans. Comput. Imag.*, vol. 7, pp. 713–723, 2021.

[18] A. Christ et al., "The virtual family development of surface based anatomical models of two adults and two children for dosimetric simulations," *Phys. Med. Biol.*, vol. 55, no. 2, pp. 23–38, 2010.

[19] C. Collins and M. Smith, "Signal-to-noise ratio and absorbed power as functions of main magnetic field strength, and definition of "90°" RF pulse for the head in the birdcage coil," *Magn. Reson. Med.*, vol. 45, no. 4, pp. 684–691, 2001.

[20] P. S. Fuchs, S. Mandija, P. R. S. Stijnman, W. M. Brink, C. A. T. van den Berg, and R. F. Remis, "First-order induced current density imaging and electrical properties tomography in MRI," *IEEE Trans. Comput. Imag.*, vol. 4, no. 4, pp. 624–631, Dec. 2018.

[21] R. Leijsen, W. Brink, X. An, A. Webb, and R. Remis, "Transverse-EPT: A local first order electrical properties tomography approach not requiring estimation of the incident fields," *Prog. Electromagn. Res. M*, vol. 102, pp. 137–148, 2021.

[22] R. Leijsen, W. Brink, C. van den Berg, A. Webb, and R. Remis, "3-D contrast source inversion-electrical properties tomography," *IEEE Trans. Med. Imag.*, vol. 37, no. 9, pp. 2080–2089, Sep. 2018.

[23] P. R. S. Stijnman, S. Mandija, P. S. Fuchs, C. A. T. van den Berg, and R. F. Remis, "Transceive phase corrected 2D contrast source inversion-electrical properties tomography," *Magn. Reson. Med.*, vol. 85, no. 5, pp. 2856–2868, 2021.